JACS
JOURNAL OF THE AMERICAN CHEMICAL SOCIETY
pubs.acs.org/JACS
Article

Chimeric Biocatalyst Combining Peptidic and Nucleic Acid Components Overcomes the Performance and Limitations of the Native Horseradish Peroxidase

Xiaobo Zhang,[‖] Dehui Qiu,[‖] Jielin Chen, Yue Zhang, Jiawei Wang, Desheng Chen, Yuan Liu, Mingpan Cheng, David Monchaud, Jean-Louis Mergny, Huangxian Ju, and Jun Zhou*

Cite This: J. Am. Chem. Soc. 2023, 145, 4517−4526

Read Online

ACCESS | Metrics & More | Article Recommendations | Supporting Information

ABSTRACT: Chimeric peptide-DNAzyme (CPDzyme) is a novel artificial peroxidase that relies on the covalent assembly of DNA, peptides, and an enzyme cofactor in a single scaffold. An accurate control of the assembly of these different partners allows for the design of the CPDzyme prototype G4-Hemin-KHRRH, found to be >2000-fold more active (in terms of conversion number k_{cat}) than the corresponding but non-covalent G4/Hemin complex and, more importantly, >1.5-fold more active than the corresponding native peroxidase (horseradish peroxidase) when considering a single catalytic center. This unique performance originates in a series of gradual improvements, thanks to an accurate selection and arrangement of the different components of the CPDzyme, in order to benefit from synergistic interactions between them. The optimized prototype G4-Hemin-KHRRH is efficient and robust as it can be used under a wide range of non-physiologically relevant conditions [organic solvents, high temperature (95 °C), and in a wide range of pH (from 2 to 10)], thus compensating for the shortcomings of the natural enzymes. Our approach thus opens broad prospects for the design of ever more efficient artificial enzymes.

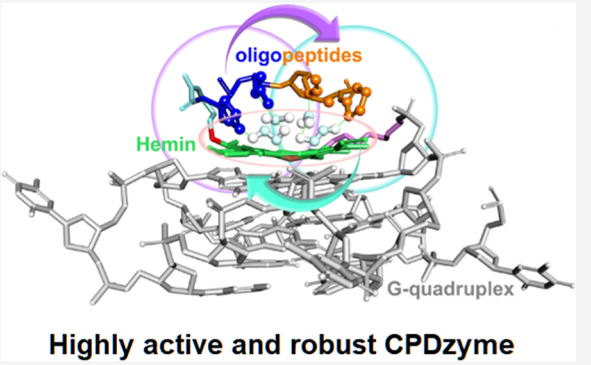

INTRODUCTION

Scientists are devising different strategies to circumvent the deficiency of native enzymes, yet highly efficient but intrinsically fragile, including, for instance, directed evolution[1−3] or enzyme immobilization.[4,5] Another strategy currently in the limelight is the design and use of artificial enzymes. The structure of native enzymes, including not only proteinaceous enzymes but also nucleic acid-based DNAzymes and ribozymes, relies on a handful of building blocks only, that is, amino acids, nucleotides, and redox molecules.[6−10] The recent advances in the development of more efficient artificial enzymes stemmed from a deeper understanding of the catalytic mechanism of native enzymes[7,11] and the application of this knowledge to recreate high-performance catalytic sites in synthetic biocatalysts.[12−14]

The usual routes to construct biomimetic enzymes rely either on the chemical optimization of naturally occurring catalysts[15−17] or on the design of new artificial catalysts based on the structural insights gained from studying the enzyme active sites.[18−20] A typical example of this approach is the development of horseradish peroxidase (HRP) surrogates:[13] HRP is a hemoprotein (i.e., containing a heme prosthetic group) that is a well-established molecular tool for ELISA assays, immunohistochemical investigations, and immunoblotting analyses. Besides protein engineering[21−26] and de novo design of enzyme mimics,[27−33] a well-known HRP-mimicking system is the G-quadruplex/hemin DNAzyme, originating in the association of a peculiar four-stranded DNA structure (G-quadruplex) with the HRP cofactor hemin. Alternative efforts have also been invested to provide hemin with a binding site in which it can be catalytically activated using, for example, self-assembled peptides in the aim of encapsulating the catalytic center from the external deactivating aqueous environment[34,35] or facilitating new catalytic reactions.[36] These studies highlighted the potential of DNA and/or peptide building blocks to design artificial enzymatic systems, whose additional interest resides in their structural modularity via a well-established chemistry. This led us to envision that combining DNA and peptidic building blocks around the hemin cofactor within a single scaffold could provide an unprecedently active artificial peroxidase.

Received: October 27, 2022
Published: February 16, 2023

https://doi.org/10.1021/jacs.2c11318
J. Am. Chem. Soc. 2023, 145, 4517−4526

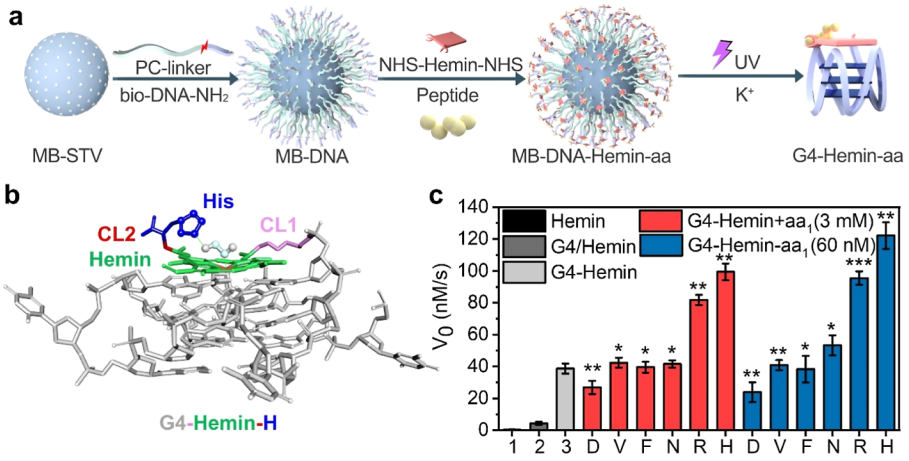

Figure 1. Synthesis, illustration, and amino acid screening of CPDzymes. (a) Schematic representation of the preparation of the CPDzyme (G4-Hemin-amino acid) and (b) of the structure of G4-Hemin-H, with a highlight of the covalent links between the G-quadruplex and hemin (pink, CL1) and hemin and His (red, CL2). (c) Comparison of catalytic activity of non-covalent vs covalent systems: H_2O_2-promoted oxidation of ABTS catalyzed by hemin alone (1), hemin in the presence of the G-quadruplex (G4/Hemin, 2), covalently linked G4-Hemin (60 nM, 3), G4-Hemin (60 nM) in the presence of various amino acids (3 mM, red bars), and the covalent assembly of G4-Hemin-aa (60 nM, blue bars). Student's *t*-tests are performed between G4-Hemin and corresponding CPDzymes: $*p \leq 0.05$; $**p \leq 0.01$; and $***p \leq 0.001$.

However, a bottleneck in the design of nature-inspired catalysts stands in the difficulty to recreate the highly complex three-dimensional organization of the enzyme active site. Some recently developed building blocks have expanded the possibility uniquely provided by mimetic enzymes:[18,20,37] for example, efforts were made to recreate and then optimize the hemin-iron catalytic center, boosting its activity by introducing additional ancillary iron-chelating moieties,[38−40] which opens ways toward new applications,[12,41] yet at the expense of an easy chemical access.[17,42−45] In fact, this long-standing quest has provided interesting artificial catalysts, although no system relying on a single catalytic site actually competes with natural enzymes.

We took up and met this challenge here, introducing a system named chimeric peptide-DNAzyme (CPDzyme), whose design hinges on a strategy in which finely selected building blocks are positioned in an optimized arrangement. This design relies on a combination of the building blocks described above (G-quadruplex, hemin, and either amino acids or oligopeptides) within a single scaffold, in a controlled arrangement, thanks to the covalent links created between the different blocks. The best CPDzyme prototype, named G4-Hemin-KHRRH, surpasses HRP in k_{cat} (when considering a single catalytic site), thus establishing a new landmark in the artificial enzyme field. Its superiority over HRP was further substantiated by its implementation in reactions performed under harsh conditions such as high temperature (up to 95 °C), extreme pH (from 2 to 10), and non-aqueous media, which is precluded for HRP. This work thus provides a new design of artificial metalloenzymes and opens up a brand new field of industrially relevant applications.

RESULTS

Preparation of CPDzymes. CPDzymes are devised as artificial catalysts that must be easily prepared and purified. To this end, our approach relied on the dissymmetric modification of the two carboxylate arms of hemin and on an on-bead synthesis strategy using the streptavidin-coated magnetic bead (MB-STV) to avoid time consumption and laborious synthesis and purification (Figure 1a). First, MB-STV was used to connect the chemically modified DNA sequence containing G-quadruplex-forming sequence (detailed in Table S1). For example, the sequence biotin-T_9/iPCLink/T$\underline{G_3TG_3TG_3TG_3}$-$NH_2$, termed bio-PC-G4-$NH_2$ (the G-quadruplex-forming sequence is underlined), is biotinylated on its 5′ end to be immobilized on the MB via STV-biotin association, while its 3′ end is modified by an amino group to allow for hemin linkage via an amide bond coupling. The other carboxylic arm of hemin is coupled to either amino acids or oligopeptides (see below), and the resulting CPDzyme is freed by UV irradiation, which cuts the internal photocleavage site (iPCLink). The main procedure of CPDzyme preparation is schematically represented in Figure 1a, and the full details are provided in the Materials and Methods section below. It should be noted that the STV molecule is a tetrameric protein with a size of 66 kDa, and the loading ratio precludes contacts between individual G4s once bound to the surface.[46] After CPDzyme isolation, its G-quadruplex is properly folded by the addition of K^+, confirmed by fluorescence titrations with thiazole orange (Figure S1).[47] A schematic representation of the CPDzyme is seen in Figure 1b, in which both carboxylate arms of hemin (green) are coupled with the folded G-quadruplex structure (gray) on one side and an amino acid (here, a histidine, in blue) on the other side.

The actual concentration of the CPDzyme was evaluated by UV−vis absorption of hemin and confirmed by an independent technique in which the peptides were replaced by DOTA-Gd to evaluate the bead loading by ICP−MS analysis (Figure S2). As seen in Figure S3, UV spectra indicated that 100 ng/mL MBs could be loaded with 308 nM CPDzymes, and this result was in agreement with the data obtained by ICP−MS (1 ng/mL MBs contains ca. 3 nM CPDzymes). Furthermore, the successful syntheses of G4-Hemin and two representative CPDzymes discussed below were confirmed by mass spectrometric characterization (Figure S4). As each CPDzyme displays a single catalytic center, its catalytic activity can therefore be directly compared to that of HRP that contains a single catalytic center as well.

Desymmetrization of Hemin and Screening of Building Blocks. It is difficult to recreate the environment

https://doi.org/10.1021/jacs.2c11318
J. Am. Chem. Soc. 2023, 145, 4517−4526

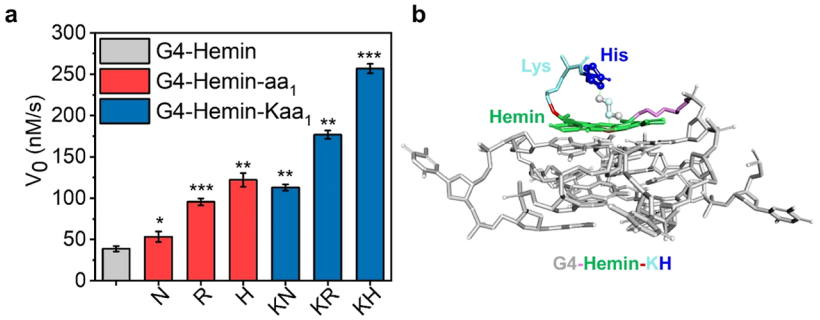

Figure 2. Embedding a lysine in the CPDzyme scaffold improves its catalytic activity. (a) Effect of the Lys (K) spacer on the catalytic activity (H_2O_2-promoted ABTS oxidation) in CPDzymes, estimated by G4-Hemin-aa$_1$ (red bars) vs G4-Hemin-Kaa$_1$ (blue bars). N, R, and H stand for asparagine, arginine, and histidine, respectively. Note: G4-Hemin activity shown for comparison. (b) Schematic representation of the structure of G4-Hemin-KH, where the Lys (light blue) serves as a spacer between His and hemin. Student's *t*-tests are performed between G4-Hemin and corresponding CPDzymes: $*p \leq 0.05$; $**p \leq 0.01$; and $***p \leq 0.001$.

of hemin within the HRP structure as it is tightly wrapped in an intricate amino acid network. This is why we decided to fully exploit the two carboxylate groups of hemin as they can constitute the bridges necessary to introduce suited blocks (Figure 1b), that is, the G-quadruplex via the covalent link 1 (CL1, pink, the 3′ end of DNA being modified with a C_6-NH_2 tail that is covalently linked to hemin upon activation as a NHS ester, Figure S5) and the oligopeptide (whose nature will be further discussed hereafter) via the covalent link 2 (CL2, red; via the naturally occurring NH_2 of amino acids, Figure S5). The catalytic activity of CPDzymes was evaluated by the model oxidation reaction of 2,2′-azino-bis(3-ethylbenzothiazoline-6-sulfonic acid) (ABTS) in the presence of the stoichiometric amounts of oxidant H_2O_2.[48−50] The initial velocity (V_0) of the ABTS oxidation under various conditions is displayed in Figure 1c; these results, in line with previous observations,[51,52] confirm that covalently linking the G-quadruplex and hemin (G4-Hemin, light gray bars) results in a better catalytic system (8.8-fold enhancement) than the non-covalent G4/Hemin assembly (dark gray bars).

Next, the amino acid blocks were screened. As seen in Figures 1c and S6, the presence of an excess of amino acid (3 mM) affects the catalytic performances of G4-Hemin (60 nM) as a function of their nature: the negatively charged aspartate (Asp, D) slightly decreases the catalysis efficiency (red bar, D) and the neutral valine (Val, V), phenylalanine (Phe, F), and asparagine (Asn, N) have no effects (red bars V, F and N), while the positively charged arginine (Arg, R) and histidine (His, H) significantly enhance the catalytic activity (2.5- and 3.2-fold, red bars R and H, respectively), in line with the highly conserved amino acids in native enzymes.[52,53] Interestingly, the strategy of covalently linking amino acids to G4-Hemin provides an efficient catalytic system as the performance of 60 nM G4-Hemin-aa$_1$ (blue bars) reaches that of 60 nM G4-Hemin + 3 mM amino acid (red bars). The most efficient systems comprised positively charged Arg and His.

Synergistic Relationship between the Different Building Blocks. It is known that cytosine, which was already used as a surrogate for HRP's distal His, must be positioned at an optimal distance from the catalytic center to be operative (which was again confirmed by the observations shown in Figure S7).[43,45] We decided to increase the distance between the Arg/His amino acids and the hemin using lysine (Lys, K) as a bridge because its side chain is flexible and long enough to facilitate the proper orientation of the co-catalytic blocks. As seen in Figures 2a and S8, embedding a Lys in the CPDzyme scaffold improved its catalytic activity by ca. 2-fold. The best result was obtained with G4-Hemin-KH (Figure 2b): the Lys might enable the His to act as in the native enzyme, that is, to coordinate H_2O_2 right above the iron atom of hemin, thus facilitating the production of compound I.[54−56]

Next, positively charged Arg and His were used to keep on improving the performance of CPDzymes (Figures 3a and S9a). First, the simultaneous introduction of two histidines did not further improve the catalytic capacity of CPDzymes (G4-Hemin-KH vs G4-Hemin-KHH) (Figure 3a). Interesting effects could nevertheless be obtained by combining His and Arg: the best combination was G4-Hemin-KHR (V_0 = 432 ±

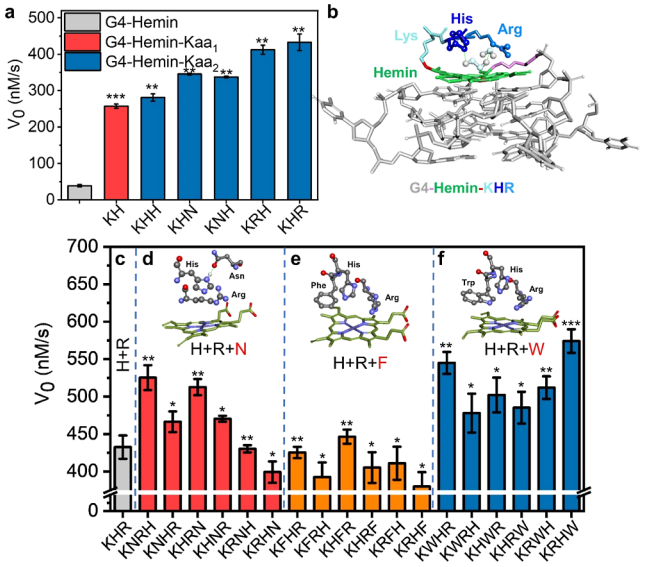

Figure 3. Biomimetic and synergistic catalytic design of CPDzymes. (a) Effect of two-membered amino acid arms on the catalytic activity (H_2O_2-promoted ABTS oxidation) of CPDzymes. Note: G4-Hemin activity shown for comparison. Student's *t*-tests are performed between G4-Hemin and corresponding CPDzymes: $*p \leq 0.05$; $**p \leq 0.01$; and $***p \leq 0.001$. (b) Schematic representation of the structure of G4-Hemin-KHR, in which Arg (blue) assists His (dark blue) in coordinating H_2O_2. (c−f) Effect of three-membered amino acid arms on the catalytic activity of CPDzymes (with His and Arg in positions 1 and 2, respectively). For comparison, the activity of G4-Hemin-KHR showed in panels a and c. Student's *t*-tests are performed between G4-Hemin-KHR and corresponding CPDzymes : $*p \leq 0.05$; $**p \leq 0.01$; and $***p \leq 0.001$.

https://doi.org/10.1021/jacs.2c11318
J. Am. Chem. Soc. 2023, 145, 4517−4526

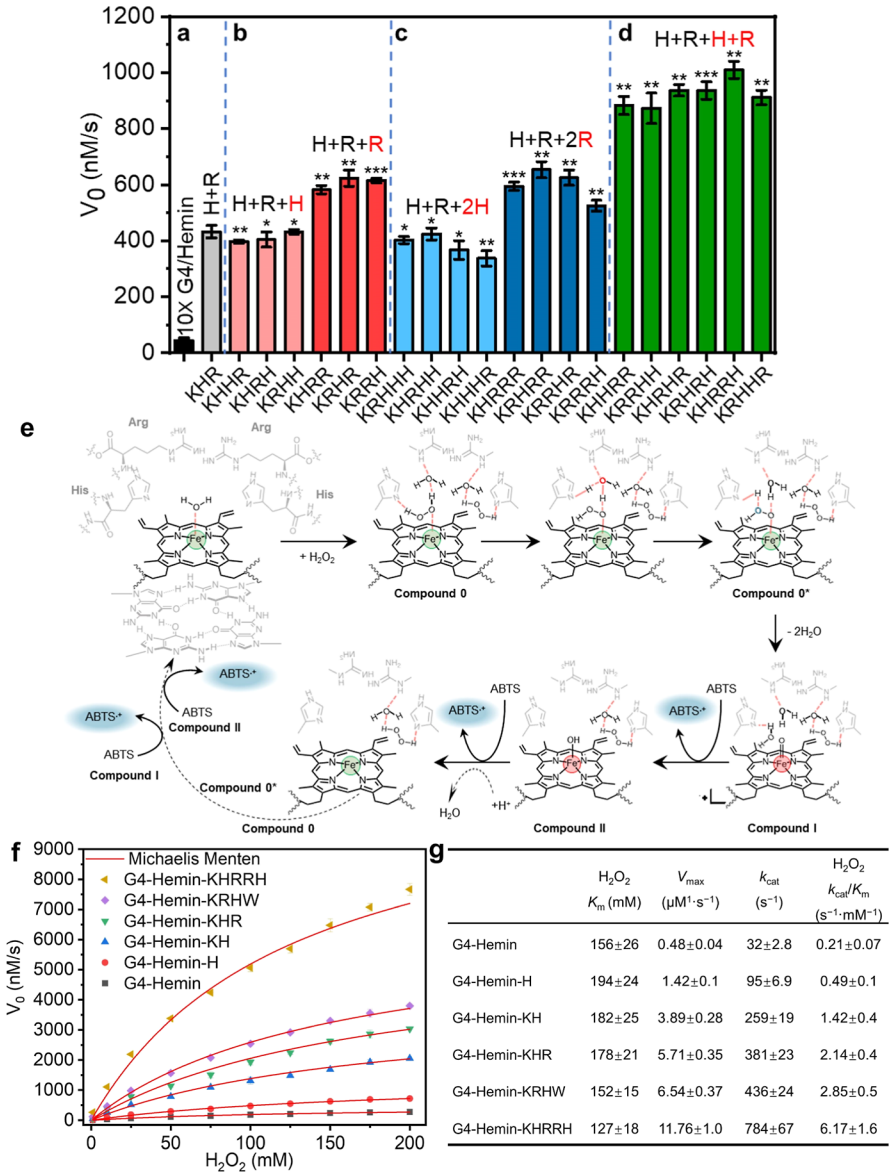

g

	H_2O_2 K_m (mM)	V_{max} (μM·s^{-1})	k_{cat} (s^{-1})	H_2O_2 k_{cat}/K_m (s^{-1}·mM^{-1})
G4-Hemin	156±26	0.48±0.04	32±2.8	0.21±0.07
G4-Hemin-H	194±24	1.42±0.1	95±6.9	0.49±0.1
G4-Hemin-KH	182±25	3.89±0.28	259±19	1.42±0.4
G4-Hemin-KHR	178±21	5.71±0.35	381±23	2.14±0.4
G4-Hemin-KRHW	152±15	6.54±0.37	436±24	2.85±0.5
G4-Hemin-KHRRH	127±18	11.76±1.0	784±67	6.17±1.6

Figure 4. Artificial synergistic catalytic design, proposed rotational catalytic mechanism, and kinetics of CPDzymes. (a–d) Effect of multiple-membered amino acid arms on the catalytic activity (H_2O_2-promoted ABTS oxidation) of CPDzymes in which G4-Hemin-K is added of (b) 2H and R, or H and 2R, (c) 3H and R, or H and 3R, and (d) 2H + 2R. Notes: the corresponding activity of G4/Hemin, is 10× magnified (a) for the sake of comparison. Student's *t*-tests are performed between G4-Hemin-KHR and corresponding CPDzymes: $*p \leq 0.05$; $**p \leq 0.01$; and $***p \leq 0.001$. (e) Schematic representation of the catalytic cycle of G4-Hemin-KHRRH for the oxidation of ABTS by H_2O_2. Green and red spheres represent Fe(III) and Fe(IV), respectively. (f) Saturation curves corresponding to the ABTS oxidation by G4-Hemin without or with peptide ancillary arms (H, KH, KHR, KRHW, and KHRRH) at different concentrations of H_2O_2 and (g) corresponding kinetic parameters. Experiments were performed in 10 mM Tris–HCl buffer (pH 7, 100 mM K^+) containing 15 nM CPDzymes and 5 mM ABTS.

15 nM/s, Figure 3a,b), which might originate from the ability of Arg to create a positive microenvironment that favors the formation of compound I.[7,9,11] Previous site-directed mutation studies have indeed demonstrated that the mutation of Arg in the native enzyme results in the loss of its catalytic activity, highlighting the important role of Arg from an evolution perspective.[57,58] The proposed structure of Hemin-KHR displayed in Figure 3b reflects what is commonly found in native peroxidases,[59,60] demonstrating that the concomitant presence of His and Arg, along with their precise organization in space, makes them synergistically interact to improve the catalytic efficiency of the resulting CPDzyme.

To go a step further, a close inspection of the structures of the peroxidases HRP and cytochrome c peroxidase (CcP) (PDB IDs: 1W4Y and 4CVJ, Figure S10) allowed for selecting the next amino acid candidates. These structures indicate that not only His and Arg (vide supra) but also Asn could be used to optimize CPDzymes.[61,62] The minor difference between HRP and CcP is a Phe41 in the former and a Trp51 in the latter. As seen in Figures 3c–f and S9b, the synergy between His, Arg, and Asn is strongly position-dependent: the best catalytic systems include continuous Arg and His and the presence of a spacer between His and Asn. This phenomenon implied that Asn needs to be accurately positioned to form hydrogen bonds with His (Figure 3c,d). Phe did not affect the CPDzyme performance, while Trp did, owing to its ability to be involved in H-bonds and participate in the catalytic process.[61] Therefore, Trp led to a better catalytic performance

https://doi.org/10.1021/jacs.2c11318
J. Am. Chem. Soc. 2023, 145, 4517–4526

(Figure 3c,e,f), the most optimized organization being G4-Hemin-KRHW, in which Arg and Trp were distributed on both sides of His (with V_0 = 574 ± 15 nM/s), in a manner reminiscent of the catalytic microenvironment in CcP.

Boosting CPDzyme Catalytic Efficiency by Artificial Synergistic Catalytic Design. G4-Hemin-KRHW is an efficient CPDzyme, but its activity could be still improved by further optimizing the G4-Hemin-KHR scaffold (Figure 3a,b). In this molecular organization, His acts both as a hydrogen bond partner for H_2O_2 and as an acid−base catalyst, making it the key amino acid for the initiation of the catalytic process. Further addition of His did not increase the catalytic activity (Figures 4a,b and S11), while that of Arg increased it by ca. 1.5-fold (with V_0 increasing from 432 ± 22 to 623 ± 29 nM/s). Further increasing the number of His did not enhance the catalytic activity, likely because of the lack of Arg to assist the catalysis of newly added His (e.g., the close activities of KHR, KHRH, and KHRHH systems). In contrast, Arg may facilitate the reaction likely via the formation and stabilization of compound I, allowing for reaching a V_0 value of ca. 600 nM/s with G4-Hemin-KHR + 2R (Figure 4c). The coordination of H_2O_2 seemed to be central to the HRP activity: H_2O_2 must be present near the catalytic site and both His and Arg can help position it close to hemin. We further explored the effect of combinations formed by two His and two Arg on the activity of the CPDzymes: the activities of systems with two sets of His/Arg combinations were ca. 2-fold better than systems with a single set of His/Arg combination (Figure 4d). Also, the catalytic performance was better when the two His were separated by Arg (i.e., HRHR, RHRH, HRRH > HHRR, RRHH, RHHR). The catalytic activity of G4-Hemin-KHRRH, with two HR pairs in mirror-inverted configuration, increased to 1009 ± 30 nM/s (Figure 4d), significantly higher than that of G4-Hemin-KRHW (V_0 = 574 ± 15 nM/s). This result led us to propose the catalytic mechanism seen in Figure 4e: the two H_2O_2 are captured by two HR pairs and then delivered to hemin in a sequential manner, providing hemin with a double fuel system that allows for considerably increasing the velocity and efficiency of the whole system.

Further increasing the length of peptide arms of G4-Hemin-KHRRH with H, R, HR, and RH combinations did not improve the efficiency of the catalysis (Figure S12), suggesting that the space within the catalytic center is limited. It is important to highlight that the G-quadruplex structure plays a central role in the catalysis (hemin coordination), as demonstrated by the significant decrease in the catalysis efficiency when the G-quadruplex-forming sequence was replaced by the control oligothymidylate T16 (Figure S13). Finally, we demonstrated that the catalytic proficiency of these CPDzymes was not substrate-dependent, as similar trends were observed with different substrates (Figure S14) including 3,3′,5,5′-tetramethylbenzidine (TMB), dopamine and nicotinamide adenine dinucleotide (NADH) (Figure S15), luminol, and Amplex Red (Figure S16) along with a series of organic dyes (further discussed below).

Kinetic Analyses and Comparison with HRP. To gain more insights into the way CPDzymes catalyze oxidation reactions, notably in comparison with the native HRP, the steady-state kinetics of Michaelis−Menten curves were investigated after each round of optimization. First, the catalytic number (k_{cat}) of HRP used herein is 521 s^{-1} at pH 4.3 (Figure S17), which is in agreement with reported values.[63−65] As displayed in Figure 4f,g, the k_{cat} value of G4-Hemin (32 s^{-1}) was better than that of the non-covalent G4/Hemin system (0.3 s^{-1}),[42] highlighting the benefit of CL1. The k_{cat} of the smallest CPDzyme, that is, G4-Hemin-H, was also better (95 s^{-1}), which highlighted the benefit of CL2. The introduction of a Lys residue as a spacer boosted the k_{cat} of G4-Hemin-KH to 259 s^{-1}, demonstrating the critical role of a precise spatial organization. A combination of His and Arg further improved the k_{cat} of G4-Hemin-KHR to 381 s^{-1}, confirming the synergistic interaction of the HR pair. The introduction of additional amino acids made the resulting CPDzyme even closer to HRP used herein (the k_{cat} value of G4-Hemin-KRHW is 436 s^{-1}). Finally, the k_{cat} of G4-Hemin-KHRRH, whose design relies on a combination of HR pairs, reached 784 s^{-1}, which is about 1.5-fold higher than that of HRP, thus representing an unprecedented catalytic performance, found to be 2600-fold higher than the non-covalent G4/Hemin system. These results reflect the catalytic synergy that can be reached by combining the G-quadruplex, hemin, and oligopeptides in a single scaffold. The other catalytic parameters (K_m and k_{cat}/K_m values, Figure 4g) confirmed the exquisite performance of G4-Hemin-KHRRH; for example, K_m values gradually deceased from 194 mM for G4-Hemin-H to 127 mM for G4-Hemin-KHRRH, and the corresponding k_{cat}/K_m values increased from 0.49 to 6.17 s^{-1} mM^{-1}. Of note, these analyses were based on the variations of the H_2O_2 concentrations; we also varied the concentrations of ABTS, and the collected results (Figure S18) confirmed that CPDzyme's efficiency is substrate-independent.

CPDzymes Are More Practically Convenient Than HRP. We demonstrated that G4-Hemin-KHRRH outperforms HRP under conditions in which the optimal enzymatic activity is ensured. We next assessed whether CPDzymes could perform catalytic transformations under conditions that are incompatible with the use of HRP, for example, in organic solvents, high temperatures, and high/low pHs. First, G4-Hemin-KHRRH remained highly active in solutions with 50% (v/v) organic solvents (formamide, methanol, ethanol, acetone, and acetonitrile, Figures S19 and S20a), while HRP did not. The oxidative degradation of Basic Blue 9 (BB9, Figure S14) in a 1:1 methanol/H_2O solution was used as a model reaction (Figures S19a,b and S20b): the degradation of BB9 catalyzed by G4-Hemin-KHRRH reached 77.7% within 20 min, while no reaction occurred without the catalyst or with HRP. This degradation was also studied at high temperatures (Figures S19c,d and S21), with 75.9% of degradation observed within 10 min at 95 °C with G4-Hemin-KHRRH, while no reaction occurred with HRP. Interestingly, G4-Hemin-KHRRH remained active (ca. 50%) after 24 h at 95 °C, displaying an impressive temperature resistance (Figure S21). Finally, the degradation of two other dyes, acid blue 74 (AB74) and basic red 2 (BR2), was studied at pH 2 for the former and pH 10 for the latter. We first verified the catalytic capacity (ABTS oxidation) of G4-Hemin-KHRRH at pH = 2−10; results seen in Figure S22a,b showed that the CPDzyme is active over the whole pH range (with an optimal activity at pH 7), representing a significantly wider pH range than that tolerated by the HRP. Next, the degradation of AB74 was studied at pH 2 (Figure S19e,f): this degradation reached 78.5% with CPDzymes within 20 min, which was far higher than that of HRP (24.4%). Then, the degradation of BR2 was studied at pH 10 (Figure S19g,h): 42.3% of BR2 degradation was obtained with G4-Hemin-KHRRH, while no reaction was monitored with HRP. This series of results (summarized in

https://doi.org/10.1021/jacs.2c11318
J. Am. Chem. Soc. 2023, 145, 4517−4526

Table 1. Dye Degradation (%) by Different Catalysts under Various Conditions

	50% methanol[a]	95 °C[b]	pH 2[a]	pH 10[a]
background	1.0 ± 0.08	4.3 ± 0.4	1.0 ± 0.1	6.7 ± 0.6
HRP	1.4 ± 0.1	4.5 ± 0.5	24.4 ± 4.2	7.3 ± 0.7
G4-Hemin-KHRRH	77.7 ± 7.8	75.9 ± 9.8	78.5 ± 6.1	42.3 ± 7.4

[a]degradation rate within 20 min; [b]degradation rate within 10 min.

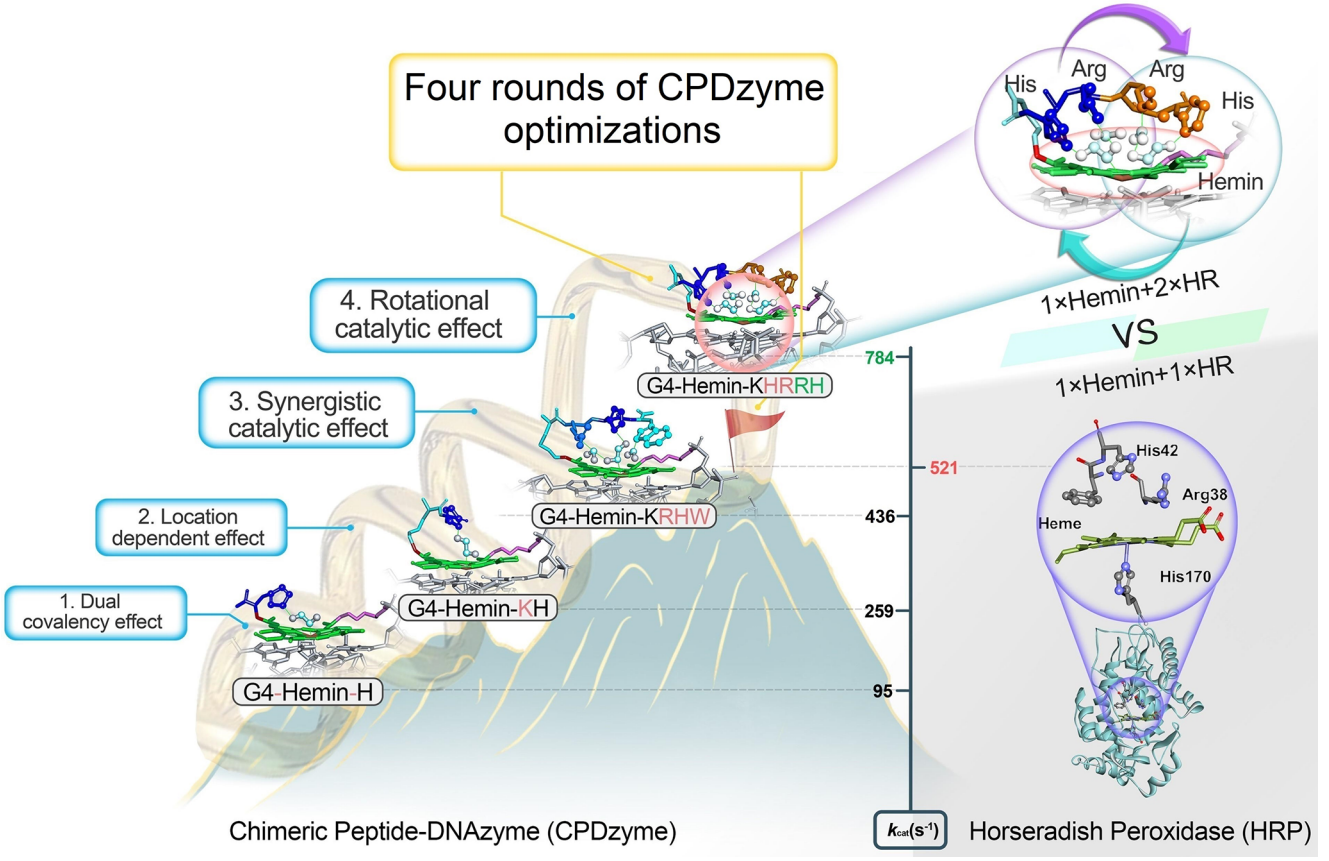

Figure 5. Catalytic efficiency of CPDzymes surpasses HRP. Schematic representation of the structure of HRP (lower right panel) vs the optimized CPDzyme G4-Hemin-KHRRH (upper right panel) and of the various rounds of optimizations that to the best CPDzyme prototype G4-Hemin-KHRRH, illustrated by a gradual increase in the k_{cat} values from 95 (G4-Hemin-H) to 259 (G4-Hemin-KH), 436 (G4-Hemin-KRHW), and 784 s^{-1} (G4-Hemin-KHRRH) vs 521 s^{-1} for HRP.

Table 1) demonstrated the superiority of CPDzymes over HRP as they can be used in a broad range of non-physiologically relevant conditions. Finally, to keep on increasing the practical convenience of CPDzymes, G4-Hemin-KHRRH was immobilized on MBs, and this conjugate was used in several rounds of ABTS oxidation. Quite satisfyingly, the resulting MB-CPDzyme had excellent stability, and its catalytic activity was >93% maintained after 10 cycles (Figure S23).

DISCUSSION

Here, we proposed the concept of the CPDzyme, a new biocatalytic system made of several building blocks (DNA, peptide, and hemin), covalently linked in a precise manner, which eventually leads to the first artificial enzyme that outperforms the corresponding natural peroxidase HRP. As summarized in Figure 5, four rounds of optimizations were required to obtain a CPDzyme able to surpass the catalytic performance of HRP. This milestone was made possible by the double covalent functionalization of hemin, along with a series of cutting edge techniques that greatly facilitate CPDzyme synthesis (Figure 1a).

In detail, the first round of optimizations was focused on the two covalent linkages CL1 and CL2 around the central hemin platform (Figure 1b). This approach allowed for gathering the G-quadruplex pre-catalyst with its cofactor hemin on one side (CL1) and the amino acid/oligopeptide activators on the other side (CL2, Figure S5). CL1 not only ensures efficient and stable hemin stacking onto the terminal G-quartet of the G-quadruplex but also solves the problem of hemin dimerization usually observed with the conventional G-quadruplex/Hemin system. CL2 provides a suitable catalytic microenvironment to hemin, close to that of HRP, playing the roles of iron auxiliary activators. Of note, although this strategy proves to be efficient, the lengths of CL1 and CL2 could be further optimized. The screening of different amino acids/oligopeptides revealed that imidazole (His)- and guanidine (Arg)-containing arms were critical for hemin activation, suggesting that the precise nature of these arms deserves to be further investigated.

https://doi.org/10.1021/jacs.2c11318
J. Am. Chem. Soc. 2023, 145, 4517−4526

The second round of optimization aimed at defining the optimal positions of the amino acid residues. We found that the introduction of a lysine on the hemin platform provided the best catalytic systems (evidenced by the significant difference between G4-Hemin-KH and G4-Hemin-H, Figure 2) likely due to its optimal length and flexibility.

Then, the effect of multi-amino acid arms on the CPDzyme performance was assessed during the third round of optimizations (Figure 5). We found that His and Arg were both critical for the transition state stability,[61] while both Asn and Trp improved the catalytic performance of CPDzymes, but in a more modest manner (Figure 3d–f).

The fourth and last round of optimizations was focused on the possible cooperativity between different amino acids pairs. This optimization led to the best CPDzyme prototype, G4-Hemin-KHRRH, which outperformed the native enzyme HRP (k_{cat}, Figure 5), thus marking a milestone in the field of mimetic enzymes. This ultimate improvement might be due to the synchronization of the two His/Arg pairs, which rotate one after the other to bring H_2O_2 close to the catalytic center, as proposed in Figure 4e. This rotational process greatly enhances the overall catalytic efficiency of the corresponding CPDzyme. It has to be noted, however, that the K_m (H_2O_2) of G4-Hemin-KHRRH lags way behind that of HRP (127 vs 0.11 mM, respectively, Figures 4g and S17d), indicating that there is still room for improvement in this catalytic design. For example, the design of an appropriate peptide to increase the binding of the CPDzyme to its substrates may further enhance the catalytic activity.[14] As an example (Figure S24), the binding study of several CPDzymes to dopamine indicated that G4-Hemin-KHRRH displays the strongest affinity, in line with its optimized activity. However, the relationship between binding ability and catalytic activity is not straightforward, which is also observed for the binding energy evaluated by docking experiments (Figures S25 and S26), suggesting that even if the binding strength is important for CPDzyme activity, it might not be the determinant factor.

In conclusion, the assembly of the three blocks, including hemin (the natural cofactor of HRP), a peculiar DNA structure referred to as a G-quadruplex (known to display high affinity for hemin and to activate its catalytic properties), and peptides (to recreate the microenvironment found in the active site of HRP), allows for the design of the CPDzyme prototypes that, after four rounds of optimizations, compete with HRP. This optimized system displays great practical advantages over HRP, being operatable under harsh experimental conditions (mixtures of organic solvents, high temperatures, high/low pHs, etc.) and easily recycled without loss of efficiency (10 cycles). We showed here the strategic relevance of CPDzyme through the oxidation of a series of dyes (BB9, AB74, and BR2), which are common pollutants found in the wastewater of the textile industry. Efforts must now be invested to gain mechanistic insights into the way CPDzymes perform their catalytic transformation, in the ultimate goal of designing more efficient systems (notably optimizing the G-quadruplex unit, which was only partly investigated here). The CPDzyme concept described here thus ensures the improvements of applications involving either hemoproteins or G-quadruplex-based DNAzyme, which are both abundant and diverse in the literature, thus representing the surest pledge for a dazzling future for nanobiocatalysis.

MATERIALS AND METHODS

Preparation of CPDzymes. As illustrated in Figure 1a, the streptavidin-coated MBs and the 10-fold excess of biotinylated DNA strands were mixed in 10 mM B&W buffer (pH 7.0, 500 μM EDTA, 1 mM K^+) and shaken at 25 °C for 3 h. MBs were then isolated by magnetic separation, rinsed (thrice), and resuspended in 10 mM HEPES (pH 7.0) buffer, and 100-fold excess of pre-mixed NHS-Hemin-NHS, amino acid/peptide, and 0.2 mg/mL DMAP (the volume of the aqueous and organic phases was adjusted to reach the 1:1 ratio) were added, and the mixture was stirred at 0 °C overnight. A magnetic separation (as mentioned above) allowed to isolate the MB-G4-Hemin-aa conjugates, which were irradiated with ultraviolet light for 30 min to free the CPDzyme (photocut molecular breakage), which was then properly folded by adding potassium to the buffer.

Measurement of CPDzyme Catalytic Activity (V_0). CPDzymes, ABTS (1 mM), and H_2O_2 (1 mM) were mixed in 10 mM Tris–HCl buffer (pH 7.0, 100 mM K^+). The catalytic activity measurement was followed by monitoring the absorbance of the oxidized ABTS ($ABTS^{\cdot+}$) which has a typical UV–vis signature at 420 nm using a Cary100 (Agilent) spectrophotometer for 60 s at 25 °C. Three other substrates, TMB, dopamine, and NADH, were also tested (see Figure S14): the absorbance of the oxidized TMB ($TMB^{\cdot+}$) is monitored at 652 nm, dopamine at 480 nm, and NADH at 340 nm, all reactions were recorded during 60 s. The extinction coefficient for $ABTS^{\cdot+}$ at 420 nm is 36,000 M^{-1} cm^{-1}; $TMB^{\cdot+}$ at 652 nm was 39,000 M^{-1} cm^{-1}; dopamine oxidation product at 480 nm is 3058 M^{-1} cm^{-1}; and NADH at 340 nm is 6220 M^{-1} cm^{-1}. The initial rate (V_0, nM/s) of the oxidation reaction was obtained from the slope of the initial linear portion (the first 5 s) of the plot of absorbance versus reaction time. All kinetic results were obtained from triplicate experiments.

Kinetic Analysis. The oxidation reaction kinetics were established using a steady-state assay, with initial reaction rates varying with the concentrations of substrates. The kinetic parameters were calculated according to the Michaelis–Menten equation: $V_0 = (V_{max} \times [S])/(K_m + [S])$, where V_0 is the initial reaction rate, V_{max} is the maximum reaction rate, [S] is the concentration of the substrate, and K_m is the Michaelis constant. $K_{cat} = V_{max}/[E_0]$ is the catalytic number, in which $[E_0]$ is the concentration of the catalyst.

ASSOCIATED CONTENT

Supporting Information

The Supporting Information is available free of charge at https://pubs.acs.org/doi/10.1021/jacs.2c11318.

Materials, reagents and methods; preparation of G4-Hemin and G4-Hemin-DOTA-Gd; additional fluorescence, UV and mass spectra; detailed structure of CPDzymes: chemical structures of Arg, His, dipeptides, key amino acid residues in the heme-binding region of HRP and CcP, and of the substrates used herein; plots of absorbance at 420 nm as a function the time; saturation curves; comparison of the catalytic activity of HRP and CPDzymes; binding affinities and energies of CPDzymes (PDF)

AUTHOR INFORMATION

Corresponding Author

Jun Zhou – *State Key Laboratory of Analytical Chemistry for Life Science, School of Chemistry & Chemical Engineering, Nanjing University, Nanjing 210023, China;* orcid.org/0000-0002-6793-3169; Email: jun.zhou@nju.edu.cn

Authors

Xiaobo Zhang – *State Key Laboratory of Analytical Chemistry for Life Science, School of Chemistry & Chemical Engineering, Nanjing University, Nanjing 210023, China;* orcid.org/0000-0003-0222-2515

https://doi.org/10.1021/jacs.2c11318
J. Am. Chem. Soc. 2023, 145, 4517–4526

Dehui Qiu − *State Key Laboratory of Analytical Chemistry for Life Science, School of Chemistry & Chemical Engineering, Nanjing University, Nanjing 210023, China*
Jielin Chen − *State Key Laboratory of Analytical Chemistry for Life Science, School of Chemistry & Chemical Engineering, Nanjing University, Nanjing 210023, China;* orcid.org/0000-0003-4930-2870
Yue Zhang − *State Key Laboratory of Analytical Chemistry for Life Science, School of Chemistry & Chemical Engineering, Nanjing University, Nanjing 210023, China*
Jiawei Wang − *State Key Laboratory of Analytical Chemistry for Life Science, School of Chemistry & Chemical Engineering, Nanjing University, Nanjing 210023, China; Laboratoire d'Optique et Biosciences (LOB), Ecole Polytechnique, CNRS, INSERM, Institut Polytechnique de Paris, 91128 Palaiseau, France*
Desheng Chen − *State Key Laboratory of Analytical Chemistry for Life Science, School of Chemistry & Chemical Engineering, Nanjing University, Nanjing 210023, China*
Yuan Liu − *State Key Laboratory of Analytical Chemistry for Life Science, School of Chemistry & Chemical Engineering, Nanjing University, Nanjing 210023, China*
Mingpan Cheng − *State Key Laboratory of Analytical Chemistry for Life Science, School of Chemistry & Chemical Engineering, Nanjing University, Nanjing 210023, China;* orcid.org/0000-0003-1282-0076
David Monchaud − *Institut de Chimie Moléculaire (ICMUB), CNRS UMR6302, UBFC, 21078 Dijon, France;* orcid.org/0000-0002-3056-9295
Jean-Louis Mergny − *State Key Laboratory of Analytical Chemistry for Life Science, School of Chemistry & Chemical Engineering, Nanjing University, Nanjing 210023, China; Laboratoire d'Optique et Biosciences (LOB), Ecole Polytechnique, CNRS, INSERM, Institut Polytechnique de Paris, 91128 Palaiseau, France;* orcid.org/0000-0003-3043-8401
Huangxian Ju − *State Key Laboratory of Analytical Chemistry for Life Science, School of Chemistry & Chemical Engineering, Nanjing University, Nanjing 210023, China;* orcid.org/0000-0002-6741-5302

Complete contact information is available at: https://pubs.acs.org/10.1021/jacs.2c11318

Author Contributions

[‖]X.Z. and D.Q. are joint first authors.

Notes

The authors declare no competing financial interest.

■ ACKNOWLEDGMENTS

The authors acknowledge the financial support of the National Natural Science Foundation of China (21977045, 22177047, 22004062, and 22104063), State Key Laboratory of Analytical Chemistry for Life Science (5431ZZXM2202 and SKLACLS2109), China Postdoctoral Science Foundation (2021M702106), and the Fundamental Research Funds for the Central Universities (202200324 and 202200325).

■ REFERENCES

(1) Coelho, P.; Brustad, E. M.; Kannan, A.; Arnold, F. H. Olefin cyclopropanation via carbene transfer catalyzed by engineered cytochrome P450 enzymes. *Science* **2013**, *339*, 307−310.
(2) Yang, K.; Wu, Z.; Arnold, F. H. Machine-learning-guided directed evolution for protein engineering. *Nat. Methods* **2019**, *16*, 687−694.
(3) Brandenberg, O.; Chen, K.; Arnold, F. H. Directed evolution of a cytochrome P450 carbene transferase for selective functionalization of cyclic compounds. *J. Am. Chem. Soc.* **2019**, *141*, 8989−8995.
(4) Grunwald, P. Immobilized biocatalysts. *Catalysts* **2018**, *8*, 386.
(5) Grigoras, A. Catalase immobilization—A review. *Biochem. Eng. J.* **2017**, *117*, 1−20.
(6) Liu, M.; Chang, D.; Li, Y. Discovery and biosensing applications of diverse RNA-cleaving DNAzymes. *Acc. Chem. Res.* **2017**, *50*, 2273−2283.
(7) Moody, P. C. E.; Raven, E. L. The nature and reactivity of ferryl heme in Compounds I and II. *Acc. Chem. Res.* **2018**, *51*, 427−435.
(8) Rawlings, N. D.; Barrett, A. J. Evolutionary families of peptidases. *Biochem. J.* **1993**, *290*, 205−218.
(9) Poulos, T. L. Heme enzyme structure and function. *Chem. Rev.* **2014**, *114*, 3919−3962.
(10) Fedor, M. J.; Williamson, J. R. The catalytic diversity of RNAs. *Nat. Rev. Mol. Cell Biol.* **2005**, *6*, 399−412.
(11) Gumiero, A.; Metcalfe, C. L.; Pearson, A. R.; Raven, E. L.; Moody, P. C. E. Nature of the ferryl heme in Compounds I and II. *J. Biol. Chem.* **2011**, *286*, 1260−1268.
(12) Wang, F.; Lu, C.; Willner, H. I. From cascaded catalytic nucleic acids to enzyme-DNA nanostructures: controlling reactivity, sensing, logic operations, and assembly of complex structures. *Chem. Rev.* **2014**, *114*, 2881−2941.
(13) Travascio, P.; Li, Y.; Sen, D. DNA-enhanced peroxidase activity of a DNA aptamer-hemin complex. *Chem. Biol.* **1998**, *5*, 505−517.
(14) Golub, E.; Albada, H. B.; Liao, W. C.; Biniuri, Y.; Willner, I. Nucleoapzymes: Hemin/G-quadruplex DNAzyme-aptamer binding site conjugates with superior enzyme-like catalytic functions. *J. Am. Chem. Soc.* **2016**, *138*, 164−172.
(15) Travascio, P.; Bennet, A. J.; Wang, D. Y.; Sen, D. A ribozyme and a catalytic DNA with peroxidase activity: active sites versus cofactor-binding sites. *Chem. Biol.* **1999**, *6*, 779−787.
(16) Ponce-Salvatierra, A.; Wawrzyniak-Turek, K.; Steuerwald, U.; Höbartner, C.; Pena, V. Crystal structure of a DNA catalyst. *Nature* **2016**, *529*, 231−234.
(17) Li, W.; Li, Y.; Liu, Z.; Lin, B.; Yi, H.; Xu, F.; Nie, Z.; Yao, S. Insight into G-quadruplex-hemin DNAzyme/RNAzyme: adjacent adenine as the intramolecular species for remarkable enhancement of enzymatic activity. *Nucleic Acids Res.* **2016**, *44*, 7373−7384.
(18) Lemon, C. M.; Marletta, M. A. Designer heme proteins: achieving novel function with abiological heme analogues. *Acc. Chem. Res.* **2021**, *54*, 4565−4575.
(19) Prier, C. K.; Arnold, F. H. Chemomimetic biocatalysis: exploiting the synthetic potential of cofactor-dependent enzymes to create new catalysts. *J. Am. Chem. Soc.* **2015**, *137*, 13992−14006.
(20) Taylor, A. I.; Pinheiro, V. B.; Smola, M. J.; Morgunov, A. S.; Peak-Chew, S.; Cozens, C.; Weeks, K. W.; Herdewijn, P.; Holliger, P. Catalysts from synthetic genetic polymers. *Nature* **2015**, *518*, 427−430.
(21) Oohora, K.; Onoda, A.; Hayashi, T. Hemoproteins reconstituted with artificial metal complexes as biohybrid catalysts. *Acc. Chem. Res.* **2019**, *52*, 945−954.
(22) Kleingardner, J. G.; Bren, K. L. Biological significance and applications of heme c proteins and peptides. *Acc. Chem. Res.* **2015**, *48*, 1845−1852.
(23) Kariyawasam, K.; Di Meo, T.; Hammerer, F.; Valerio-Lepiniec, M.; Sciortino, G.; Maréchal, J. D.; Minard, P.; Mahy, J. P.; Urvoas, A.; Ricoux, R. An artificial hemoprotein with inducible peroxidase- and monooxygenase-like activities. *Chem.—Eur. J.* **2020**, *26*, 14929−14937.
(24) Yin, L.; Yuan, H.; Liu, C.; He, B.; Gao, S.; Wen, G.; Tan, X.; Lin, Y. A rationally designed myoglobin exhibits a catalytic dehalogenation efficiency more than 1000-fold that of a native dehaloperoxidase. *ACS Catal.* **2018**, *8*, 9619−9624.

(25) Carminati, D. M.; Fasan, R. Stereoselective cyclopropanation of electron-deficient olefins with a cofactor redesigned carbene transferase featuring radical reactivity. *ACS Catal.* **2019**, *9*, 9683−9697.
(26) Pott, M.; Hayashi, T.; Mori, T.; Mittl, P. R. E.; Green, A. P.; Hilvert, D. A noncanonical proximal heme ligand affords an efficient peroxidase in a globin fold. *J. Am. Chem. Soc.* **2018**, *140*, 1535−1543.
(27) Koebke, K. J.; Pinter, T. B. J.; Pitts, W. C.; Pecoraro, V. L. Catalysis and electron transfer in De Novo designed metalloproteins. *Chem. Rev.* **2022**, *122*, 12046−12109.
(28) Ghirlanda, G.; Osyczka, A.; Liu, W.; Antolovich, M.; Smith, K. M.; Dutton, P. L.; Wand, A. J.; DeGrado, W. F. De novo design of a D2-symmetrical protein that reproduces the diheme four-helix bundle in cytochrome bc1. *J. Am. Chem. Soc.* **2004**, *126*, 8141−8147.
(29) D'Souza, A.; Bhattacharjya, S. De novo-designed β-sheet heme proteins. *Biochemistry* **2021**, *60*, 431−439.
(30) Hindson, S. A.; Bunzel, H. A.; Frank, B.; Svistunenko, D. A.; Williams, C.; van der Kamp, M. W.; Mulholland, A. J.; Pudney, C. R.; Anderson, J. L. Rigidifying a De Novo enzyme increases activity and induces a negative activation heat capacity. *ACS Catal.* **2021**, *11*, 11532−11541.
(31) D'Souza, A.; Wu, X.; Yeow, E. K. L.; Bhattacharjya, S. Designed heme-cage β-sheet miniproteins. *Angew. Chem., Int. Ed.* **2017**, *56*, 5904−5908.
(32) Guo, W.-J.; Xu, J.-K.; Wu, S.-T.; Gao, S.-Q.; Wen, G.-B.; Tan, X.; Lin, Y.-W. Design and engineering of an efficient peroxidase using myoglobin for dye decolorization and lignin bioconversion. *Int. J. Mol. Sci.* **2022**, *23*, 413.
(33) Nastri, F.; Chino, M.; Maglio, O.; Bhagi-Damodaran, A.; Lu, Y.; Lombardi, A. Design and engineering of artificial oxygen-activating metalloenzymes. *Chem. Soc. Rev.* **2016**, *45*, 5020−5054.
(34) Wang, Z.; Wang, H.; Liu, Q.; Duan, F.; Shi, X.; Ding, B. Designed self-assembly of peptides with G-quadruplex/hemin DNAzyme into nanofibrils possessing enzyme-mimicking active sites and catalytic functions. *ACS Catal.* **2018**, *8*, 7016−7024.
(35) Liu, Q.; Wang, H.; Shi, X.; Wang, Z.; Ding, B. Self-assembled DNA/peptide-based nanoparticle exhibiting synergistic enzymatic activity. *ACS Nano* **2017**, *11*, 7251−7258.
(36) Zozulia, O.; Korendovych, I. V. Semi-rationally designed short peptides self-assemble and bind hemin to promote cyclopropanation. *Angew. Chem., Int. Ed.* **2020**, *59*, 8108−8112.
(37) Huang, L.; Chen, J.; Gan, L.; Wang, J.; Dong, S. Single-atom nanozymes. *Sci. Adv.* **2019**, *5*, No. eaav5490.
(38) Cui, X.; Li, H.; Wang, Y.; Hu, Y.; Hua, L.; Li, H.; Han, X.; Liu, Q.; Yang, F.; He, L.; Chen, X.; Li, Q.; Xiao, J.; Deng, D.; Bao, X. Room-temperature methane conversion by graphene-confined single iron atoms. *Chem* **2018**, *4*, 1902−1910.
(39) Wang, L.; Zhu, C.; Xu, M.; Zhao, C.; Gu, J.; Cao, L.; Zhang, X.; Sun, Z.; Wei, S.; Zhou, W.; Li, W.; Lu, J. Boosting activity and stability of metal single-atom catalysts via regulation of coordination number and local composition. *J. Am. Chem. Soc.* **2021**, *143*, 18854−18858.
(40) Buss, J. A.; Agapie, T. Four-electron deoxygenative reductive coupling of carbon monoxide at a single metal site. *Nature* **2016**, *529*, 72−75.
(41) Gao, L.; Zhuang, J.; Nie, L.; Zhang, J.; Zhang, Y.; Gu, N.; Wang, T.; Feng, J.; Yang, D.; Perrett, S.; Yan, X. Intrinsic peroxidase-like activity of ferromagnetic nanoparticles. *Nat. Nanotechnol.* **2007**, *2*, 577−583.
(42) Chen, J.; Wang, J.; van der Lubbe, S. C. C.; Cheng, M.; Qiu, D.; Monchaud, D.; Mergny, J. L.; Guerra, C. F.; Ju, H.; Zhou, J. A push−pull mechanism helps design highly competent G-quadruplex-DNA catalysts. *CCS Chem.* **2021**, *3*, 2183−2193.
(43) Qiu, D.; Mo, J.; Liu, Y.; Zhang, J.; Cheng, Y.; Zhang, X. Effect of distance from catalytic synergy group to iron porphyrin center on activity of G-quadruplex/hemin DNAzyme. *Molecules* **2020**, *25*, 3425.
(44) Li, W.; Chen, S.; Xu, D.; Wen, Q.; Yang, T.; Liu, J. A DNA as a substrate and an enzyme: direct profiling of methyltransferase activity by cytosine methylation of a DNAzyme. *Chem.—Eur. J.* **2018**, *24*, 14500−14505.
(45) Chen, J.; Zhang, Y.; Cheng, M.; Guo, Y.; Šponer, J.; Monchaud, D.; Mergny, J. L.; Ju, H.; Zhou, J. How proximal nucleobases regulate the catalytic activity of G-quadruplex/hemin DNAzymes. *ACS Catal.* **2018**, *8*, 11352−11361.
(46) Zhang, X.; Liu, C.; Wang, H.; Wang, H.; Li, Z. Rare earth ion mediated fluorescence accumulation on a single microbead: An ultrasensitive strategy for the detection of protein kinase activity at the single-cell level. *Angew. Chem., Int. Ed.* **2015**, *54*, 15186−15190.
(47) Lubitz, I.; Zikich, D.; Kotlyar, A. Specific high-affinity binding of thiazole orange to triplex and G-quadruplex DNA. *Biochemistry* **2010**, *49*, 3567−3574.
(48) Wei, H.; Wang, E. Nanomaterials with enzyme-like characteristics (nanozymes): next-generation artificial enzymes. *Chem. Soc. Rev.* **2013**, *42*, 6060−6093.
(49) Kadnikova, E. N.; Kostić, N. M. Oxidation of ABTS by hydrogen peroxide catalyzed by horseradish peroxidase encapsulated into sol−gel glass: Effects of glass matrix on reactivity. *J. Mol. Catal. B: Enzym.* **2002**, *18*, 39−48.
(50) Chen, Q.; Liang, C.; Sun, X.; Chen, J.; Yang, Z.; Zhao, H.; Feng, L.; Liu, Z. H_2O_2-responsive liposomal nanoprobe for photoacoustic inflammation imaging and tumor theranostics via in vivo chromogenic assay. *Proc. Natl. Acad. Sci. U.S.A.* **2017**, *114*, 5343−5348.
(51) Mergny, J. L.; Sen, D. DNA quadruple helices in nanotechnology. *Chem. Rev.* **2019**, *119*, 6290−6325.
(52) Chen, Y.; Qiu, D.; Zhang, X.; Liu, Y.; Cheng, M.; Lei, J.; Mergny, J. L.; Ju, H.; Zhou, J. Highly sensitive biosensing applications of a magnetically immobilizable covalent G-quadruplex-hemin DNAzyme catalytic system. *Anal. Chem.* **2022**, *94*, 2212−2219.
(53) Qi, C.; Zhang, N.; Yan, J.; Liu, X.; Bing, T.; Mei, H.; Shangguan, D. Activity enhancement of G-quadruplex/hemin DNAzyme by spermine. *RSC Adv.* **2014**, *4*, 1441−1448.
(54) Howes, B. D.; Rodriguez-Lopez, J. N.; Smith, A. T.; Smulevich, G. Mutation of distal residues of horseradish peroxidase: influence on substrate binding and cavity properties. *Biochemistry* **1997**, *36*, 1532−1543.
(55) Poulos, T. L.; Kraut, J. The stereochemistry of peroxidase catalysis. *J. Biol. Chem.* **1980**, *255*, 8199−8205.
(56) Vidossich, P.; Fiorin, G.; Alfonso-Prieto, M.; Derat, E.; Shaik, S.; Rovira, C. On the role of water in peroxidase catalysis: a theoretical investigation of HRP Compound I formation. *J. Phys. Chem. B* **2010**, *114*, 5161−5169.
(57) Vitello, L. B.; Erman, J. E.; Miller, M. A.; Wang, J.; Kraut, J. Effect of arginine-48 replacement on the reaction between cytochrome C peroxidase and hydrogen peroxide. *Biochemistry* **1993**, *32*, 9807−9818.
(58) Rodriguez-Lopez, J. N.; Smith, A. T.; Thorneley, R. N. F. Role of arginine38 in horseradish peroxidase: a critical residue for substrate binding and catalysis. *J. Biol. Chem.* **1996**, *271*, 4023−4030.
(59) Groves, J. T.; Boaz, C. Fishing for peroxidase protons. *Science* **2014**, *345*, 142−143.
(60) Berglund, G. I.; Carlsson, G. H.; Smith, A. T.; Szöke, H.; Henriksen, A.; Hajdu, J. The catalytic pathway of horseradish peroxidase at high resolution. *Nature* **2002**, *417*, 463−468.
(61) Veitch, N. C. Horseradish peroxidase: a modern view of a classic enzyme. *Phytochem* **2004**, *65*, 249−259.
(62) Satterlee, J. D.; Alam, S. L.; Mauro, J. M.; Erman, J. E.; Poulos, T. L. The effect of the Asn82 to Asp mutation in yeast cytochrome c peroxidase studied by proton NMR spectroscopy. *Eur. J. Biochem.* **1994**, *224*, 81−87.
(63) Rodríguez-López, J. N.; Gilabert, M. A.; Tudela, J.; Thorneley, R. N.; García-Cánovas, F. Reactivity of horseradish peroxidase compound II toward substrates: kinetic evidence for a two-step mechanism. *Biochemistry* **2000**, *39*, 13201−13209.
(64) Fruk, L.; Müller, J.; Niemeyer, C. M. Kinetic analysis of semisynthetic peroxidase enzymes containing a covalent DNA-heme adduct as the cofactor. *Chem.—Eur. J.* **2006**, *12*, 7448−7457.

https://doi.org/10.1021/jacs.2c11318
J. Am. Chem. Soc. 2023, 145, 4517−4526

(65) Kamal, J. K.; Behere, D. V. Activity, stability and conformational flexibility of seed coat soybean peroxidase. *J. Inorg. Biochem.* **2003**, *94*, 236−242.

https://doi.org/10.1021/jacs.2c11318
J. Am. Chem. Soc. 2023, 145, 4517−4526